OncoTargets and Therapy

Dovepress
Taylor & Francis Group

Open Access Full Text Article

ORIGINAL RESEARCH

Decoding the Prognosis-Related S100A9^{high} Monocyte in Glioblastoma Using Single-Cell and Spatial Transcriptome Sequencing

Xiucan Li[1,2], Ying Qin[3], Pengfei Gao[2], Huixue Wang[2], Yanling Liu[4], Lian Ren[5], Dongdong Wu[6], Xueyuan Heng[2]

[1]Guangzhou University of Chinese Medicine, Guangzhou, Guangdong Province, People's Republic of China; [2]Department of Orthopedics, Linyi People's Hospital, Linyi, Shandong Province, People's Republic of China; [3]Department of Gastroenterology, Hospital of Traditional Chinese Medicine of Linyi City, Linyi, Shandong Province, People's Republic of China; [4]Department of General Medicine, Linyi People's Hospital, Linyi, Shandong Province, People's Republic of China; [5]Graduate School, Dalian Medical University, Dalian, Liaoning Province, People's Republic of China; [6]Chinese PLA General Hospital, Beijing, People's Republic of China

Correspondence: Xueyuan Heng, Department of Orthopedics, Linyi People's Hospital, Linyi, Shandong Province, People's Republic of China, Tel +86-13608990919, Email hengxueyuan123@126.com

Purpose: Monocytes and macrophages are recognized as predominant immune populations in human glioblastoma, where they play vital roles in tumor progression. Despite their established significance, the heterogeneity of these cells—particularly within the monocyte compartment—remains incompletely characterized.

Methods: We comprehensively used scRNA-seq, spatial transcriptome sequencing combined with immunofluorescence and T cell co-culture assays to illuminate the heterogeneity and function of monocyte in glioblastoma.

Results: In this study, from the perspective of ligand-receptor networks, we have identified and characterized three distinct glioblastoma subtypes. Single-cell RNA-seq analysis further revealed that the C3 subtype with bad prognosis exhibited a higher proportion of S100A9^{high} monocytes. Spatial transcriptomics combined with immunofluorescence assays demonstrated that these S100A9^{high} monocytes were spatially adjacent to M2 macrophages, exhausted CD8+ T cells, and endothelial cells. In vitro T cell co-culture assays revealed S100A9^{high} monocyte produced elevated levels of the immunosuppressive cytokine IL-10, reactive oxygen species (ROS) and inducible nitric oxide synthase (iNOS), all of which might impair T cell function and immune response. Notably, elevated abundance of S100A9^{high} monocyte correlated with poor patient prognosis.

Conclusion: In summary, our results deciphered the heterogeneity of monocytes in glioblastoma and identified a novel poor prognosis-associated monocyte subset, S100A9^{high} monocytes, which foster an immunosuppressive, pro-tumorigenic microenvironment.

Keywords: tumor associated monocyte, glioblastoma, immune environment, scRNA-seq, spatial transcriptome sequencing

Introduction

Glioma are the most common primary tumors in the brain and spinal cord and remain incurable. In 2007, the World Health Organization (WHO) classified tumors of the central nervous system into four WHO classes I to IV.[1] Of these, glioblastoma multiforme, or glioblastoma (GBM), is the most heterogeneous and malignant type of glioma, and even with aggressive treatment, the median survival of patients is currently only about 15 months.

The suppressive tumor microenvironment (TME) of glioblastoma is an important cause of malignant progression and treatment resistance, and the suppressive TME is mainly composed of immunosuppressive immune cells such as tumor associated myeloid cells and regulatory T cells.[2] They promote T cell apoptosis and exhaustion, and induce an immunosuppressive microenvironment, which in turn contributes to glioblastoma progression. However, due to current technical limitations, the understanding of the characteristics of the immune microenvironment of glioblastoma remains relatively limited. Deciphering the complex immune microenvironment and intertumoral heterogeneity in glioblastoma is

Received: 11 July 2025
Accepted: 24 October 2025
Published: 5 November 2025

critical not only for understanding the mechanisms underlying tumorigenesis and progression, but also for identifying novel immunotherapeutic targets and developing therapeutic approaches.

In recent years, the advent and rapid evolution of single-cell multi-omics technologies have revolutionized the dissection of immune cell heterogeneity under both homeostatic and disease conditions, providing unprecedented molecular resolution.[3–5] New glioblastoma markers have been identified with the help of single-cell transcriptome sequencing, and these new targets provide an important rationale for clinical therapeutic strategies and drug target development.[6] Importantly, using single-cell transcriptome sequencing and bioinformatics analysis, we are able to more precisely resolve the heterogeneity of the immune microenvironment cells of glioblastoma at single-cell resolution and delineate the key molecular signaling pathway as well as gene regulatory networks in play, which paves the way for a more systematic and precise understanding of heterogeneity of glioblastoma patients.[7,8] In addition, single-cell transcriptome sequencing further provides unprecedented resolution to dissect intercellular crosstalk within the tumor microenvironment and delineate its underlying molecular circuitry, thereby advancing our mechanistic comprehension of glioblastoma pathophysiological evolution and informing the development of next-generation multimodal therapeutic regimens.[5,9,10]

Collectively, in this study, we identified the novel immunosuppressive monocyte sub-population as well as the potential signaling pathway of their immunoregulatory function. These findings are expected to provide new ideas and theoretical basis for the precision treatment of glioblastoma.

Materials and Methods

Acquisition and Processing of TCGA Data

RNA-seq data for glioblastoma as well as survival-related data were obtained from the UCSC Xena database (https://xena.ucsc.edu/), which contains survival data for 649 patients as well as gene expression data for 173 patients, and patients with only both expression data and survival data were retained for subsequent analysis, with a total of 167 patients were finally used for subsequent analysis.

Hierarchical Clustering Analysis

First, we obtained ligand and receptor genes from published data, then we utilized the "hclust" function to perform hierarchical clustering analysis with setting cluster method as "ward.D2", and ultimately identified three glioblastoma subgroups with significant differences in ligand and receptor gene expression patterns.[11]

Survival Analysis

Survival analysis was performed using the "Surv" function in the survival package in R. The "ggsurvplot" function in the survminer package was used to visualize the data. For the prognostic analysis of S100hi_Mono, the top 50 signature genes of S100hi_Mono were got following differentially expressed genes(DEGs) analysis, which were further subjected to gsva scoring analysis. Then all the patients were further divided into high and low groups based on the S100hi_Mono score and used for survival analysis.

Principal Component Analysis (PCA) and T-Distributed Stochastic Neighbor Embedding (T-SNE) Analysis

To visualize the three glioblastoma groups, PCA and t-SNE analysis were performed. Firstly, we screened the top 2000 high variable genes that were significantly different between patients based on the variance of the genes, and then we used princomp package to perform PCA and the Rtsne package to perform t-SNE analysis, and then we used ggplot2 to visualize the results of the PCA and t-SNE analysis.

Differential Expression Analysis

DEGs among the three groups of patients were calculated using the limma package using "one vs all" method. P values were corrected using FDR, and all genes with adjusted P-values less than 0.05 were used for subsequent visualization and further enrichment analysis. DEGs were visualized using the "pheatmap" function in the Pheatmap package.

Functional Enrichment Analysis

We utilized the clusterProfiler package for GO enrichment analysis for the DEGs, Go terms with P values less than 0.05 were retained and subjected to visualization using ggplot2 package in R.[12]

Gene Sets Scoring

Firstly, thirteen tumor state related gene sets were downloaded from CancerSEA database, HALLMARK gene sets were downloaded from Msigdb database (https://www.gsea-msigdb.org/) and myeloid derived suppressive cells (MDSC) related gene sets were obtained from published literature.[4] Secondly, the gene sets scores were obtaining using ssgsea method in GSVA package in R.[13] Finally, the result were visualized using heatmap via pheatmap package or box and violin plot using ggplot2 package.

Immune Microenvironment Deconvolution Analysis

In order to infer the infiltration of immune cells in the each glioblastoma patient, the deconvolution method based on transcriptomic dataset was performed using "deconvo_tme" function in the IOBR package in R with setting the method as "cibersort".[14] And the predicted cell percentage of immune cells infiltrated in different groups were visualized using the "VlnPlot" function.

Acquisition and Processing of Single-Cell Transcriptome Data

Firstly, we obtained the single-cell transcriptome data of glioblastoma from the published literature.[15] The following downstream single cell RNA-seq data analysis was performed using Seurat package in R, which mainly including the quality control of the data, normalization, HVGs detection, dimensionality reduction, and clustering analysis. The populations obtained from unsupervised clustering were subsequently annotated based on the expression of marker genes reported in previous literature and differential genes between cell clusters. DEGs detection was performed using the "FindAllMarkers" function (method = "wilcox") in Seurat.

Cell-Cell Interaction Analysis

We used CellChat software to analyze the interactions between immune cells. The main process of the analysis included the construction and initialization of CellChat objects, the inference of cellular communication networks, and the visualization of cellular communication networks.[16] We used "netVisual_circle" function to visualize the emphasis of interactions between different populations, "netAnalysis_computeCentrality" and "netAnalysis_signalingRole_network" function to analyze and visualize the roles that different cell types play in signaling. Ligand and receptor pairs screened for statistical differences between groups were visualized using the "netVisual_bubble" function.

Immunofluorescence Assay

The collected GBM samples were isolated, fixed with 4% paraformaldehyde for 2 h at 4 °C, embedded in paraffin, and sectioned at 6–8 μm with Leica RM2235. Sections were deparaffinized with ethanol of gradient concentration, then blocked in blocking solution (Zhongshan golden bridge) for 30 min at room temperature, followed by incubation with primary antibodies overnight at 4 °C. After 3 washes (3 min each) in PBS, sections were incubated with corresponding secondary antibodies (Zhongshan golden bridge) for 30 min at room temperature. After 3 washes in PBS, sections were stained with DendronFluor TSA (Histova, NEON 4-color IHC Kit for FFPE, NEFP450, 1:100, 20–60 s). The primary and secondary antibodies were thoroughly eluted by heating the slides in citrate buffer (pH 6.0) for 20 min at 95 °C using microwave. Serially, each antigen was labeled by distinct fluorophores. After all the antibodies were detected sequentially, the slices were finally stained with DAPI. Images were collected by confocal microscope (Nikon Ti-E A1/ ZEISS LSM 880). The primary antibodies: CD31 (Abcam, ab182981), S100A9 (CST, D5O6O), CD8 (Abcam, ab237709), PD1 (Abcam, ab237728), MARCO (Abcam, ab239369), MANNOSE (Abcam, ab64693).

Fluorescence Activated Cell Sorting

CD45-BV421 (BD, 563879), CD14-BV786 (BD, 561712), CD300e-PE (Invitrogen, PA5-53324 and CD11c-APC-Cy7 (Biolegend, 337217) antibodies were used to label the digested GBM cells. Cells were incubated at 4°C with antibodies in the dark for 20 to 30 minutes. After staining, cells were washed and resuspended in PBS with 1% BSA and 2% 7-AAD (eBioscience, 2238457). The $CD45^+CD11c^+CD14^+CD300e^-$ and $CD45^+CD11c^+CD14^+CD300e^+$ population were simultaneously sorted with Aria 3 Flow Cytometer (BD Bioscience). The detailed sorting strategy was shown in results. Data were analyzed using FlowJo_V10 software.

T Cell Suppression Assay

We first isolated $CD8^+$ T cells from PB of healthy donors using the T cell isolation kit according to the manufacturer's instructions. T cells were stained with 10 μmol/ L proliferation dye eFluor™ 450 and cultured in RPMI 1640 medium containing 10% FBS, 100 IU/mL penicillin and 100 mg/mL streptomycin, 1 mM sodium pyruvate and 55 μM β-mercaptoethanol for mixed leucocyte reaction. Sorted $CD300E^+$ or $CD300^-$ monocyte were co-cultured with eFluor™ 450-labeled T cells at a 1:1 ratio in 96-well plates. After 72 h of incubation, $CD8^+$ T cell proliferation was assessed by eFluor™ 450 dilution and flow cytometry. Supernatants of co-cultures were collected to measure supernatant cytokine levels by ELISA. ROS measurements were determined using the Reactive Oxygen Species Assay Kit (Beyotime Biotechnology, China).

Enzyme-Linked Immunosorbent Assays

The culture supernatant was collected to detect the IL-2, IL-10, IFN-γlevels. The quantification of cytokines in the supernatant was performed using a human ELISA detection kit in accordance with the instructions provided by the manufacturer.

Results

Identification of Novel Immunosupressive Glioblastoma Subtype Based on Ligand and Receptor Network

Ligand and receptor genes have been reported to be key components for cell communication in tumor environment. On basis of the reported ligand and receptor genes, we perform unsupervised cluster analysis on the RNA-Seq data of glioblastoma patients in TCGA database. Hierarchical clustering revealed that these ligand and receptor genes were categorized into three gene modules, and based on the expression of these three modules, the glioblastoma patients were categorized into three groups, namely C1, C2, and C3 (Figure 1A). C1 lowly expresses all the ligand and receptor genes in all three gene modules. C2 highly expresses the ligand and receptor genes of gene module3, while C3 highly expresses the ligand and receptor genes of gene module1. Compared to C1, C2 and C3 highly expresses the ligand and receptor genes in gene module2 (Figure 1A).

By performing a survival analysis of the three newly identified subtypes of glioblastoma patients, we found that the three GBM subtypes exhibited significant survival differences, with C3 having the worst prognosis, whereas C1 and C2 had comparable prognoses (Figure 1B). To further investigate the differences in the transcriptomic profile of the three GBM subtypes, we performed GO enrichment analysis using the ligand and receptor genes enriched in the three gene modules. The results showed that gene module 1 was mainly enriched for GO terms related to cell adhesion, leukocyte chemotaxis, cell proliferation, myeloid cell migration, and organization of extracellular matrix. Gene module 2 was enriched for the JAK-STAT signaling pathway and neuropeptide signaling pathway. Gene module 3 was enriched for the neuron development-associated signaling pathway, including terms related to axon formation, axon guidance, and trans-synaptic signaling (Figure 1C).

Differences in Transcriptomic Profiles Among the Three GBM Subtypes

To comprehensively understand the difference among the three GBM subtypes, we further performed differential expression analysis. Consistently, we found that C2 highly expressed genes associated with synapse organization and

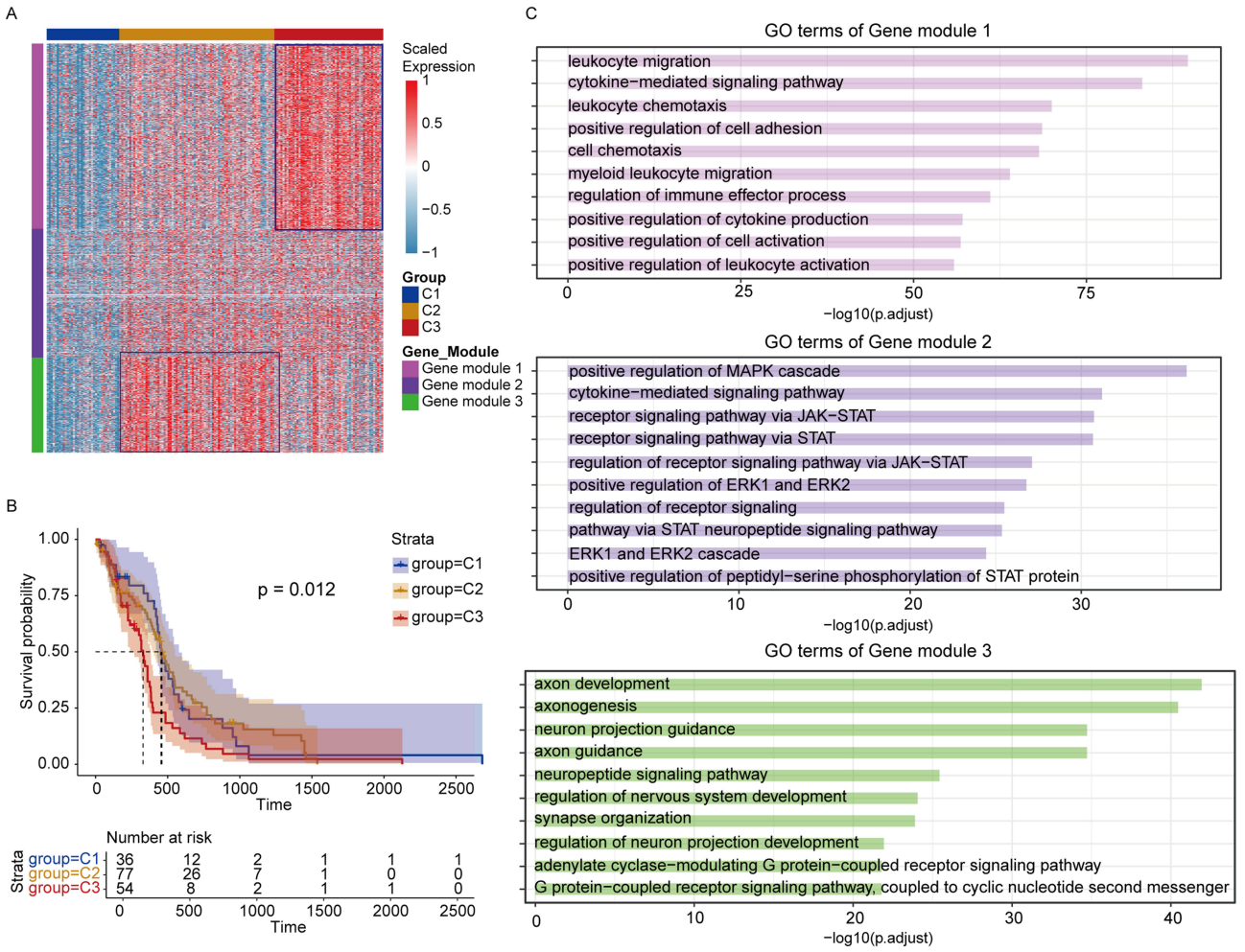

Figure 1 RNA-seq analysis on basis of ligand and receptor genes identified three GBM subtypes. (**A**) Heatmap show the expression of three gene modules in the three GBM subtypes. (**B**) Survival analysis of the three GBM subtypes. (**C**) GO terms enriched in the three gene modules.

assemble, including SPTBN2, BSN, GDAP1, and PTPN4. C3 exhibited high expression of genes associated with neutrophil activation (PLAUR, TNFRSF1B, C5AR1, LAIR1, and ALOX5), T-cell activation (RAC2, TGFBR2, and IL4R), and neutrophil degranulation (SIGLEC9 and DOK3), as well as cell adhesion-related genes such as ITGB2, ICAM1, and ITGAM. (Figure 2A and B). These GO terms derived from DEGs among the three GBM subtypes showed high consistency with those from ligand and receptor gene modules in Figure 1. Intriguingly, C3 also displayed high expression of genes associated with leukocyte chemotaxis (CCR5, CXCR4, CCR1, S100A8, IL16, C3AR1, IL6R, CCR2, and CXCL16), and immunosuppression (IL4R, IL10RA, HAVCR2, ARG1, and IL10) (Figure 2A–D), indicative of its immunosuppressive characteristics. Given that C3 highly expresses GO terms related to myeloid cells, we further investigated the expression of signature genes of the major myeloid cell lineages in the three groups. We found that C3 highly expressed the monocyte signature genes CSF1R, CD14 and FCGR3A (encoding CD16), the macrophage signature gene C1QA, and the granulocyte signature gene CSF3R (Figure 2E), which suggests an high enrichment of myeloid immune cells in C3 group.

Differences in Tumor Cell State Among the Three GBM Subtypes

In order to resolve the differences in tumor cells states of the three GBM subtypes, we evaluated fourteen functional states of the tumors using gene sets from CancerSEA database.[17] We found that the C3 group showed enhanced expression of signaling pathways associated with apoptosis, hypoxia, angiogenesis, quiescence (Figure 3A). Furthermore, C3 also highly expressed signatures related to tumor invasion, epithelial-mesenchymal transition, and

https://doi.org/10.2147/OTT.S553018

https://doi.org/10.2147/OTT.S553018

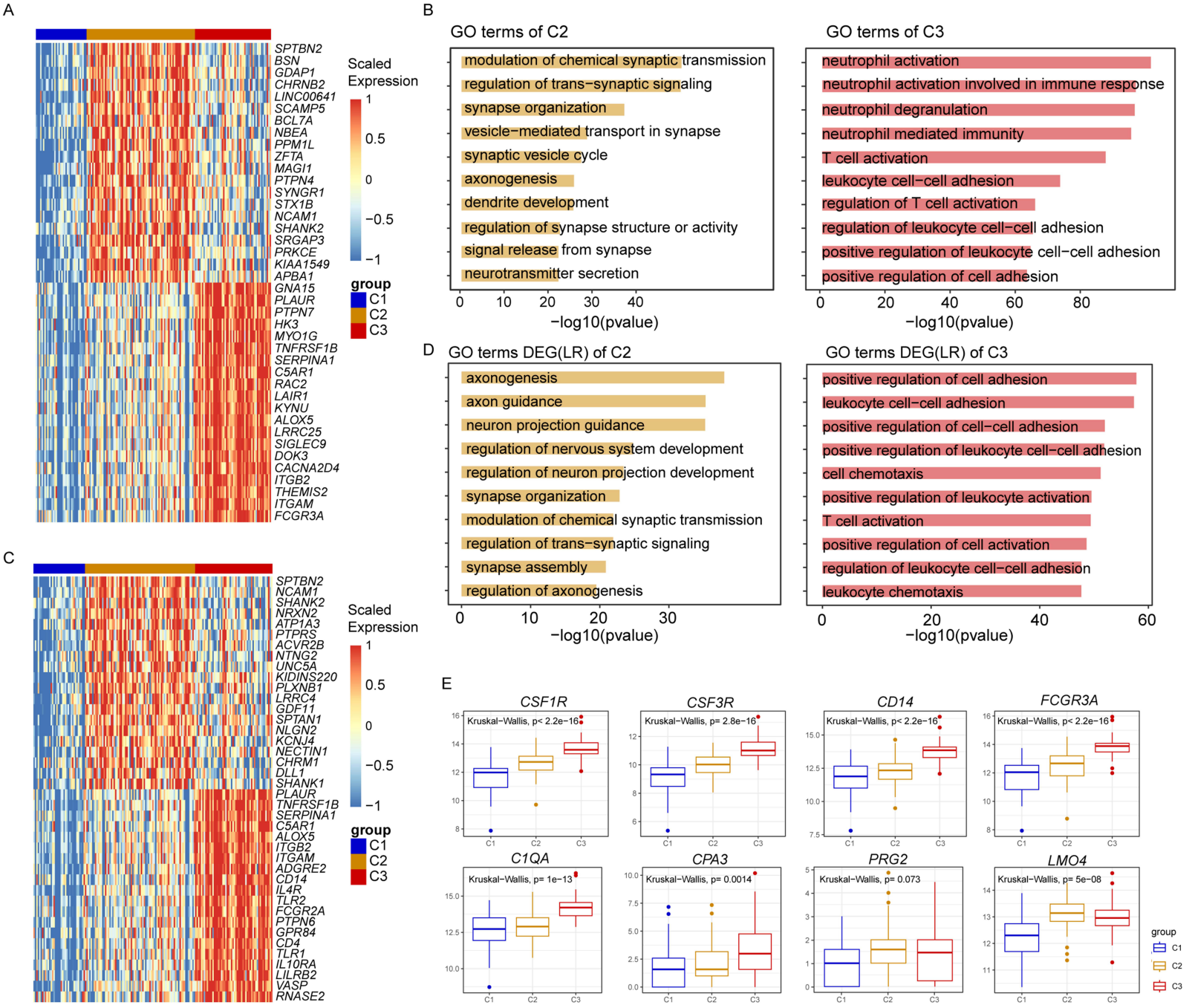

Figure 2 Difference of gene expression profile between the three GBM subtypes. (**A**) Heatmap show the DEGs between the three GBM subtypes. (**B**) GO terms enriched in three GBM subtypes using DEGs. (**C**) Differentially expressed ligand and receptor genes between the three GBM subtypes. (**D**) GO terms enriched in three GBM subtypes using ligand and receptor genes. (**E**) Box plots show the expression of myeloid immune cells associated genes.

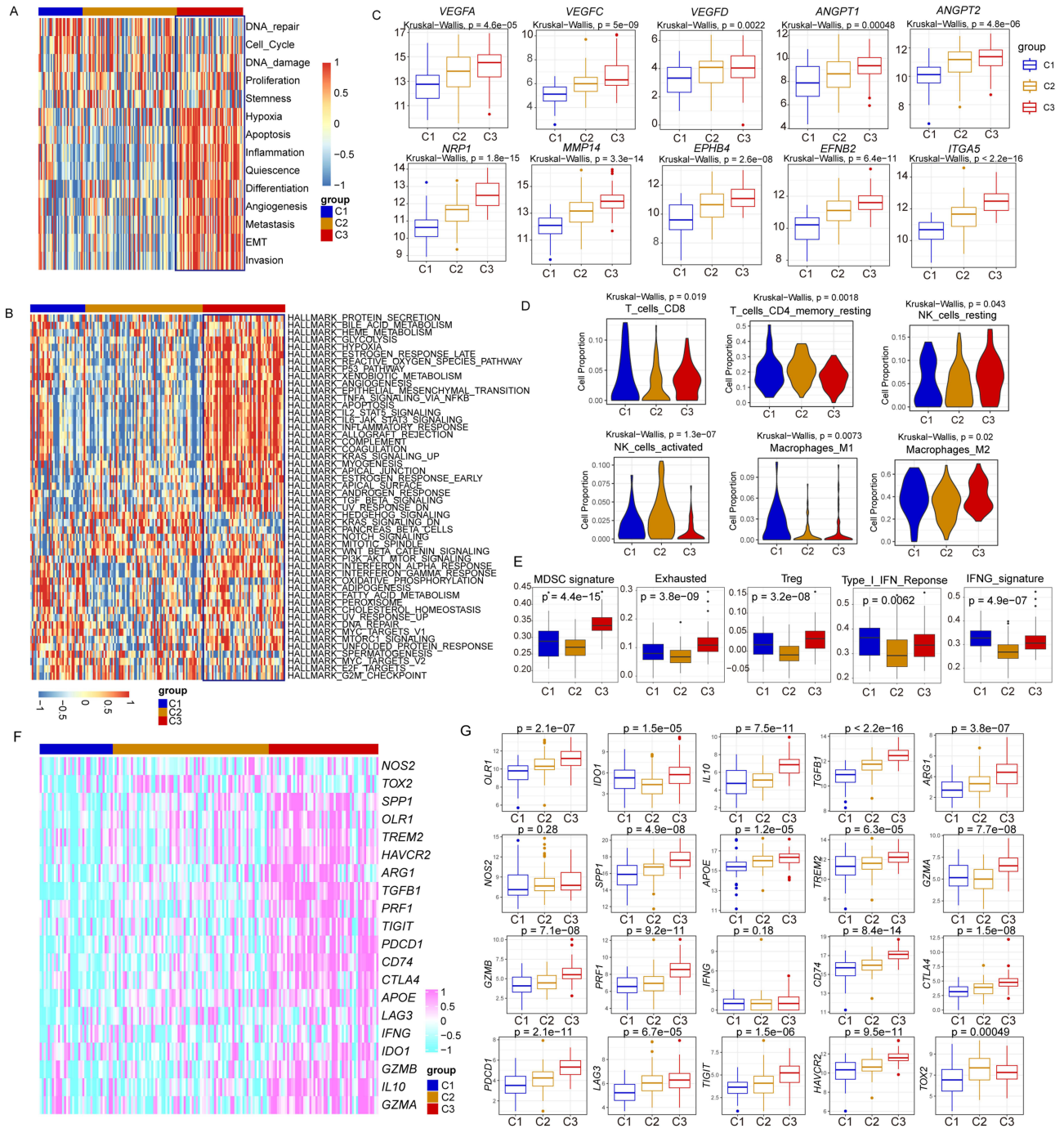

Figure 3 The difference in tumor cell state of the three GBM subtypes. (**A**) Heatmap showing the expression of 13 CancerSEA tumor cell states. (**B**) Heatmap showing the difference in expression of HALLMARK gene sets. (**C**) Box plots show the expression of angiogenesis related genes in the three GBM subtypes. (**D**) Violin plots showing the cell proportion derived from deconvolution analysis. (**E**) Box plots displaying the expression of curated immunosuppressive gene sets. (**F**) Heatmap showing the expression of immune checkpoint and exhaustion related genes. (**G**) Box plots exhibiting the expression of MDSC, and tumor associated macrophage related genes.

metastasis (Figure 3A), suggesting the highly invasive and metastatic characteristics of C3 group tumors. Next, we explored the differences in important signaling pathways among the three GBM subtypes using the classical Hallmark 50 gene sets, and our results showed that C3 exhibited higher expression of feature genes associated with glycolysis, which might attribute to the enrichment of hypoxia signaling pathway in C3 (Figure 3B). The C3 group was also enriched for angiogenesis-related pathway and genes such as VEGFA/C/D, ANGPT1 and ANGPT2, NRP1, EFNB2 and EPHB4, suggesting that C3 GBM subtype had more active angiogenesis (Figure 3B and C), which supported rapid tumor growth,

https://doi.org/10.2147/OTT.S553018

strong invasion and metastasis properties. Moreover, the C3 group expressed exhibit higher levels of P53 signaling, hedgehog signaling, and KRAS signaling (Figure 3B), all of which have reported to play roles in tumorigenesis. It is noteworthy that C3 was also enriched for TGFB signaling pathway as well as reactive oxygen species production-related signaling pathways (MPO, NQO1, SOD2, and LSP1), which have all been reported to play important roles in immunosuppression function (Figure 3B and C).[18–20] All these results suggest a immunosuppressive microenvironment of patients in C3 subtype glioblastoma.

Differences in the Immune Microenvironment Among the Three GBM Subtypes

We further delineated the differences in the tumor immune microenvironment between the three GBM subtypes using deconvolution method, and we found that the C3 group have higher percentages of $CD8^+$ T cells, resting NK cells while lower percentages of $CD4^+$ memory T cells and activated NK cells (Figure 3D). Furthermore, the C3 group have higher proportion of macrophages with M2 characteristics and a smaller proportion of macrophages with M1 characteristics relative to the C1 and C2 groups (Figure 3D). All these results further confirmed the immunosuppressive microenvironment of the C3 group. Previous studies have shown that a greater proportion of regulatory T cells (Treg), myeloid-derived suppressive cells (MDSC), as well as exhausted cytotoxic immune cells, are key features of the immunosuppressive tumor microenvironment.[21,22]

We therefore further evaluated these immunosuppressive characteristics in the three GBM subtypes and found that the C3 group exhibited higher levels of T cell exhaustion signatures, suggesting a low response status of T cells in the C3 group (Figures 3E). In addition, the C2 and C3 groups had lower levels of immune activation and inflammation-related signaling pathways compared to the C1 group, such as type I interferon responses and the IFNG signaling pathway (Figure 3E). In addition to lower percentage of inflammatory immune cells and lower expression of inflammatory signaling pathway, the C3 group was also enriched for anti-inflammatory associated immune cell populations such as Treg and MDSC (Figure 3E). We further examined the expression of key genes associated with tumor-associated macrophages (TAM) (SPP1, APOE and TREM2), MDSC (OLR1, IL10, ARG1 and IDO1), as well as immune checkpoint molecules (TIGIT, PDCD1, CTLA4, LAG3, and HAVCR2).[23] We found that all these molecules showed higher expression levels in C3 group relative to C1 and C2 groups (Figure 3F and G). Taken together, our results revealed the significant and complex immunosuppressive microenvironment in the newly identified C3 GBM subtype.

Identification of Monocyte and Macrophage Heterogeneity in Human Glioblastoma

To further understand the immunosuppressive microenvironment of glioblastoma, we integrated and reanalyzed the single-cell transcriptomic data of 4 newly diagnosed glioblastoma patients.[15] By using a graph clustering-based community detection algorithm, we identified sixteen cell types, among which eight immune cell types were identified namely monocyte (CD14, FCN1 and LYZ), macrophage and microglia (C1QB and P2RY12), conventional dendritic cell (cDC) (CLEC10A, HLA-DPA1 and HLA-DPB1), plasmacytoid dendritic cells (pDC) (IRF8, CLEC4C and IL3RA), natural killer cells (NK) (NCR1, KLRD1 and NKG7), T cell (CD3D, CD2 and CD7), and B cell (CD19, CD79A and JCHAIN) (Figures 4A–D).

We further focused on monocyte and macrophage populations, by unsupervised clustering analysis two monocyte clusters and seven macrophage sub-populations were recognized (Figure 4E). The two monocyte sub-clusters, CD52_Mono and S100hi_Mono, shared the expression of monocyte signature genes such as LYZ, FCN1 and LSP1, with the former showing higher expression of CD52 and the latter highly expressing S100A9 and S100A8. Notably, the S100hi_Mono also expressed high levels of angiogenesis gene VEGFA and epidermal growth factor ligand genes such as AREG and EREG, which have been reported to promote cell proliferation of tumor cells and induce immunosuppressive microenvironment, suggesting its important roles in occurrence and progress of glioblastoma (Figure 4F and G). Additionally, we also identified microglia and six macrophage sub-populations, including two inflammatory macrophage clusters (IFIT_Mac and Cycling_Mac) and four anti-inflammatory macrophage populations, namely AREG_Mac, MARCO_Mac, SEPP1_Mac and CCL4_Mac. GO analysis showed that anti-inflammatory macrophage clusters enriched terms associated with response to hypoxia and S100hi_Mono exhibited the enrichment of chemotaxis and immune response regulation-related terms (Figure 4H).

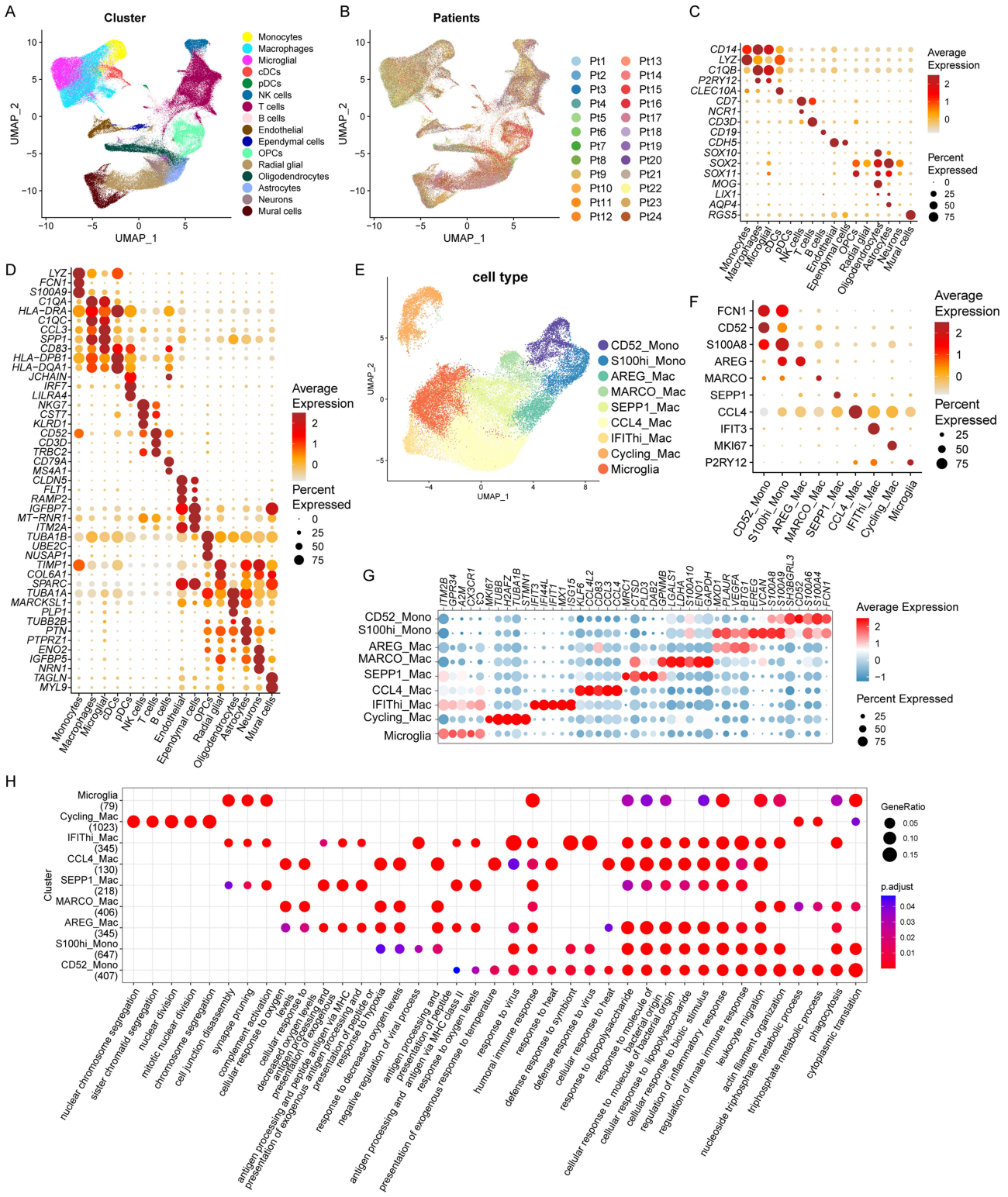

Figure 4 Monocyte and Macrophage heterogeneity in human glioblastoma. (**A**) UMAP visualization of major cell types in scRNA-seq data of human glioblastoma patients. (**B**) UMAP visualization of cells in panel with patient information mapped onto. (**C**) Dot plot showing the expression of indicated genes. (**D**) Dot plot showing the expression of top 3 DEGs for each cluster in panel A. (**E**) UMAP plot showing nine monocyte and macrophage sub-clusters with cell identities mapped onto. (**F**) Dot plot showing the feature genes used to defined cell clusters in panel E. (**G**) Dot plot showing the top 5 DEGs for cell clusters in panel E. (**H**) Dot plot showing the results of GO enrichment analysis.

https://doi.org/10.2147/OTT.S553018

The immune regulatory characteristics of S100hi_Mono inspired us to investigate the immunosuppressive role of these monocyte and macrophage clusters. To this end, we examined the expression of TAM signatures and immunosuppressive genes in these monocyte and macrophage sub-populations. We found that all the seven macrophage clusters highly expressed TAM-related genes such as SPP1, APOE and TREM2 as well as high M2 macrophage score (Figure 5A and B). Intriguingly, despite the low expression of TAM signature, S100hi_Mono showed high expression of MDSC associated genes such as OLR1 and IL1B, implying its immunosuppressive roles (Figure 5A). As expected, S100hi_Mono exhibited highest MDSC score related to other monocyte and macrophage clusters and high level of anti-inflammatory score (Figure 5B). In addition, S100hi_Mono showed high expression of angiogenesis score, suggesting its crucial role in promoting angiogenesis in tumor (Figure 5C).

To further investigate the relationship between these monocyte-macrophage sub-clusters and aforementioned poor prognostic C3 GBM subtype. We examined the expression of C3 highly expressed ligand and receptor genes (Figure 2) in these nine monocyte and macrophage clusters. We found that S100hi_Mono displayed higher expression of C3-related ligand and receptor genes, which was similar to the gene set scoring analysis (Figure 5D and E). Moreover, we further checked the expression of top 50 DEGs of S100hi_Mono in the three different GBM subtypes shown in Figure 1. The result indicated that the expression levels of these genes were higher in C3 GBM subtype, implying higher proportion of S100hi_Mono in C3 might be associated with poor prognosis of C3 GBM subtype (Figure 5F).

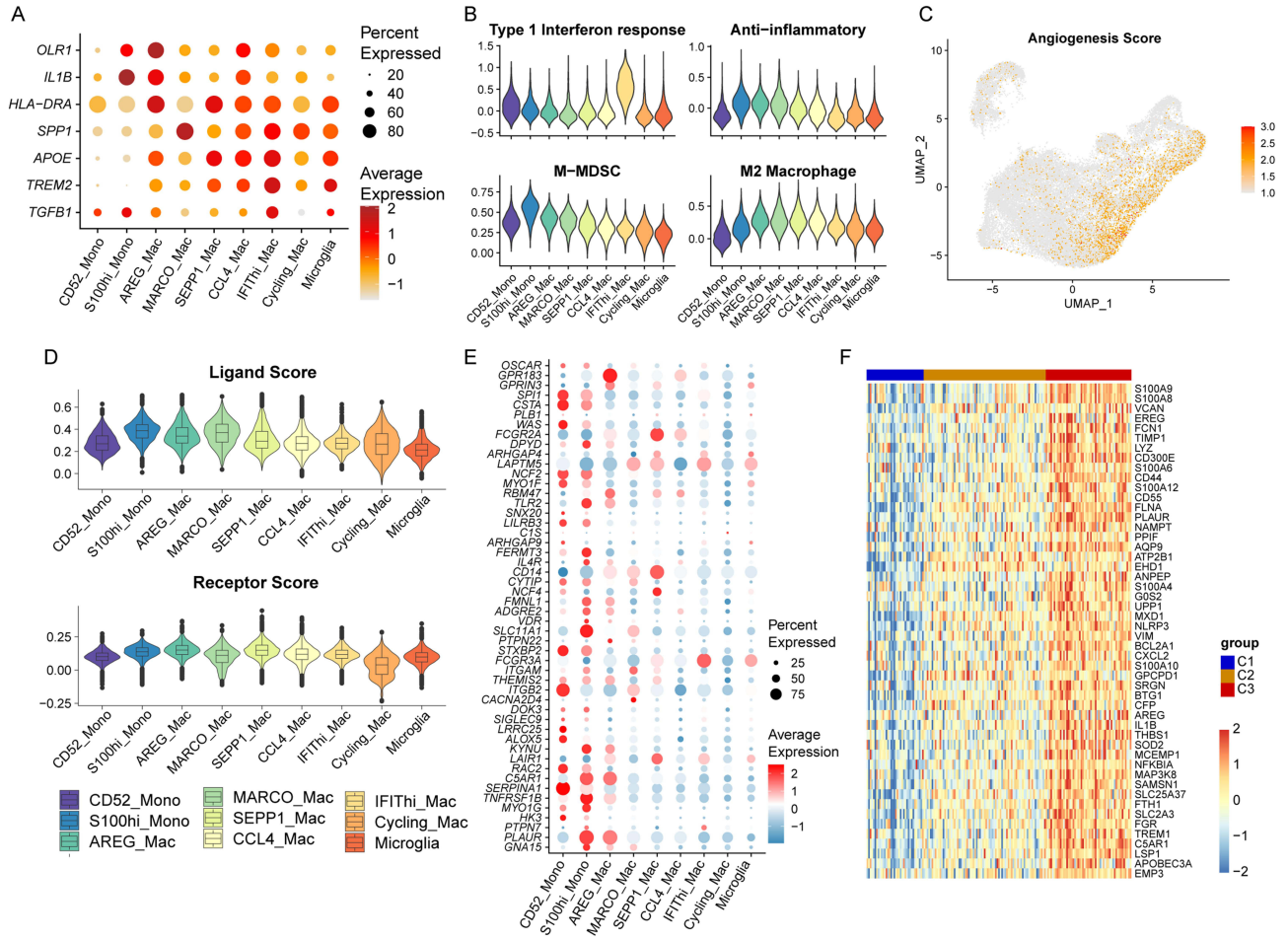

Figure 5 Immunosuppressive characteristics of the monocyte and macrophage sub-clusters. (**A**) Dot plot showing expression of TAM and MDSC related genes in nine monocyte and macrophage sub-clusters. (**B**) Violin plots showing the gene set score of Type I interferon response, anti-inflammatory, MDSC and M2 macrophage. (**C**) UMAP plot showing the angiogenesis score in all the nine monocyte and macrophage clusters. (**D**) Violin plots showing the gene set score of C3 highly expressed ligand and receptor genes. (**E**) Heatmap showing the expression of ligand and receptor genes highly expressed in C3 group. (**F**) Heatmap showing the expression of top 50 signature genes of S100hi_Mono in the three GBM subtypes.

 https://doi.org/10.2147/OTT.S553018

S100hi_Mono Promote Angiogenesis and M2 Polarization in GBM

In order to understand the cellular and molecular basis by which S100hi_Mono exerts immunosuppressive effects, we performed cell-cell interaction analysis using CellChat, and we found that the S100hi_Mono showed strong interactions with T cells, especially with CD8+ exhausted T (Figure 6A). Additionally, S100hi_Mono also exhibited strong cell communications with anti-inflammatory macrophage such as AREG_Mac and SEPP1_Mac (Figure 6A). Specifically, S100hi_Mono might recruit TAMs and CD8+ exhausted T cells via chemotaxis-related ligand and receptor pairs such as CCL3-CCR1, CCL3L3-CCR1 and CXCL16-CXCR3 (Figure 6B).

Furthermore, S100hi_Mono highly expressed M2 macrophage polarization-related ligand genes, which interacted with receptor genes expressed on the surface of TAMs. These M2 macrophage polarization associated ligand and receptor pairs include ANXA1-FPR1/FPR2/FPR3, SPP1-CD44, SPP1-(ITGAV+ITGB1), IL10-(IL10RA+IL10RB) and TGFB1-(TGFBR1+TGFBR2), all of which have been reported to be involved in M2 polarization (Figure 6B).

We further analyzed 10X Visum platform based spatial transcriptomic data of 18 newly diagnosis GBM patient samples. Cell distribution and co-location analysis revealed that the $S100A9^{high}$ monocyte was close to TAMs (MACRO_Mac), entholial cells and CD8+ exhausted T cells (Figure 6C and D). Survival analysis further revealed that patients with a high proportion of S100hi_Mono had a worse prognosis (Figure 6E). All of these indicated the immunosuppressive role of S100hi_Mono in GBM, which might induce an immune microenvironment conducive to tumors through promoting angiogenesis and M2 macrophage polarization.

T Cell Suppression Assay Validate the Immunosuppressive Function of S100hi_Mono

Next, we further investigated the immunosuppressive function of S100hi_Mono cells using a T-cell co-culture system. Differential gene expression analysis revealed that S100hi_Mono exhibited elevated surface expression of CD300E compared to other monocyte and macrophage subsets (Figure 7A). Using flow cytometry, we sorted S100hi_Mono cells (CD45+CD11c+CD300E+) and CD45+CD11c+$CD300E^{-}$ control cells for in vitro T-cell co-culture experiments (Figure 7B). The CD300E+ group (S100hi_Mono) significantly inhibited T-cell proliferation, demonstrating a lower proliferation index than positive controls ($P<0.0001$)(Figure 7C and D). Intriguingly, the $CD300E^{-}$ group also exhibited T-cell suppression, indicating the presence of other immunosuppressive myeloid cells in it (Figure 7C and D).

We next quantified inflammatory and immunosuppressive cytokines in co-culture supernatants. While both groups secreted comparable levels of pro-inflammatory cytokines such as IL-2 and IFN-γ, the CD300E+ group produced significantly higher levels of the immunosuppressive cytokine IL-10 ($P<0.05$; Figure 7E), consistent with prior cell-cell interaction data in Figure 6B. This elevated IL-10 likely contributed to suppressed T-cell cytotoxicity and promoted M2 macrophage polarization. Notably, the CD300E+ group showed enhanced generation of reactive oxygen species (ROS) and inducible nitric oxide synthase (iNOS), both of which have been reported to be involved in T-cell suppression (Figure 7F).

Collectively, these in vitro findings demonstrate that S100hi_Mono cells establish an immunosuppressive microenvironment through IL-10 production while directly impairing T-cell function via ROS and iNOS.

Discussion

Gliomas are a group of malignant tumors of the central nervous system with high heterogeneity and very poor prognosis. Classically, gliomas are classified into different subtypes according to the type of mutation in the tumor, and the most common mutations are TP53 (tumor protein 53), PTEN (phosphatase and tensin homolog), IDH1, EGFR, NF1, PIK3CA, and PIK3R1, and the clinical features and prognosis of patients harboring the different mutations are also different. Additionally, the poor prognosis of gliomas is also closely linked to its severely and complexly immunosuppressive microenvironment. Despite the vital importance of immune environment in gliomas, the current understanding of the immune ecology of gliomas is still very limited.

In recent years, the rapid development of the single-cell transcriptome as well as the spatial transcriptome have provided important technical supports and opportunities for the systematic elucidation of immune environment and signaling communication between tumor and niche cells.[5,7,24,25] Due to the presence of the blood-brain barrier, tissue-

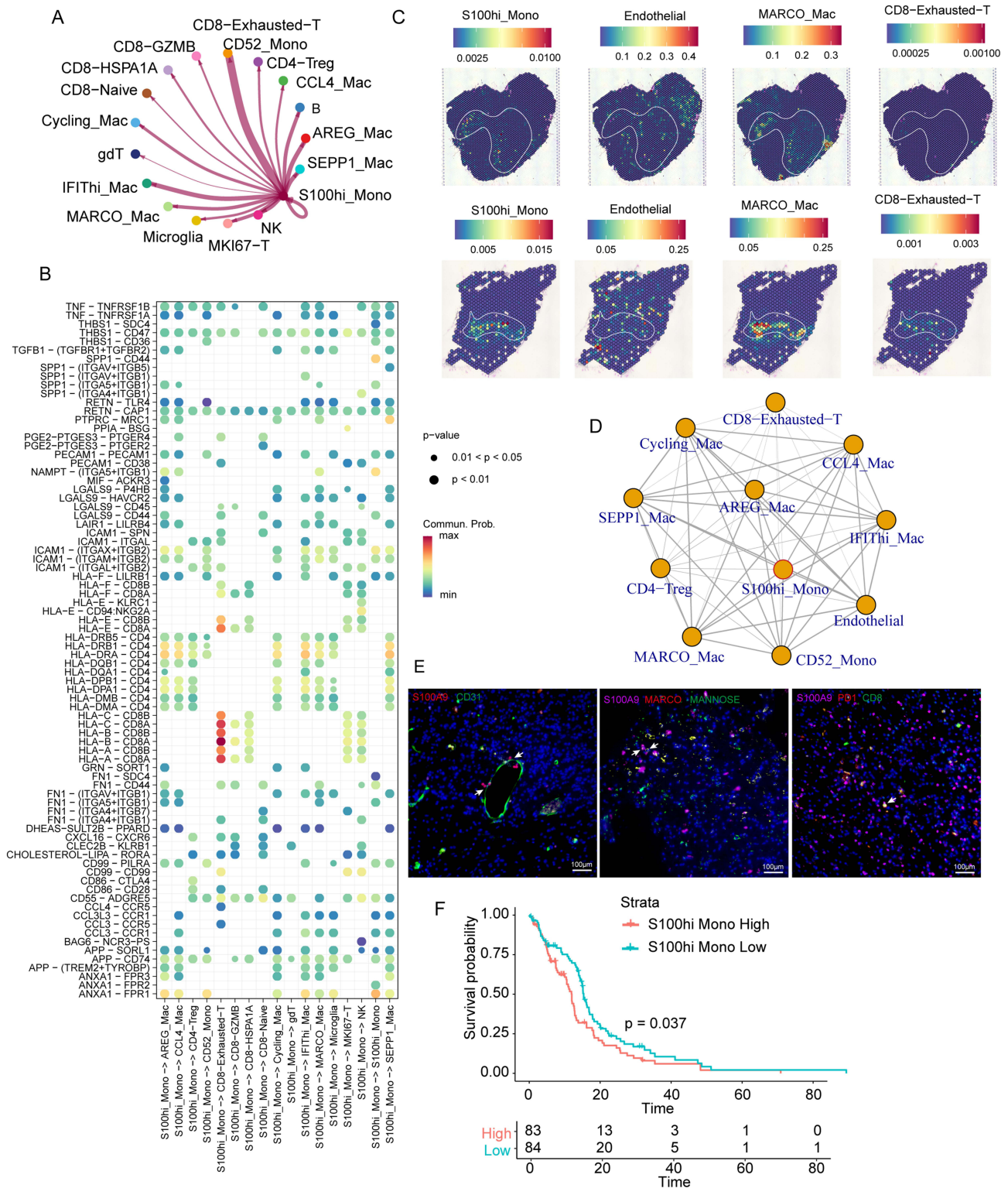

Figure 6 Cell-cell interaction analysis identified cellular and molecular basis of immunosuppressive function of S100hi_Mono. (**A**) The network showing the intensity of cell-cell interaction between different immune cell types. (**B**) Dot plot showing the differentially expressed ligand-receptor pairs in different cell type combination. (**C**) The images showing the cell proportion of indicated cell type in each spot of representative slice. (**D**) The network showing the cell co-location relationship between each cell type. The width of lines indicate intense of co-location. (**E**) Immunofluorescence assay showing the co-location between S100hi_Mono, TAM, CD8+ exhausted cells and endothelial cell. (**F**) Survival analysis of S100hi_Mono in GBM data of TCGA.

https://doi.org/10.2147/OTT.S553018

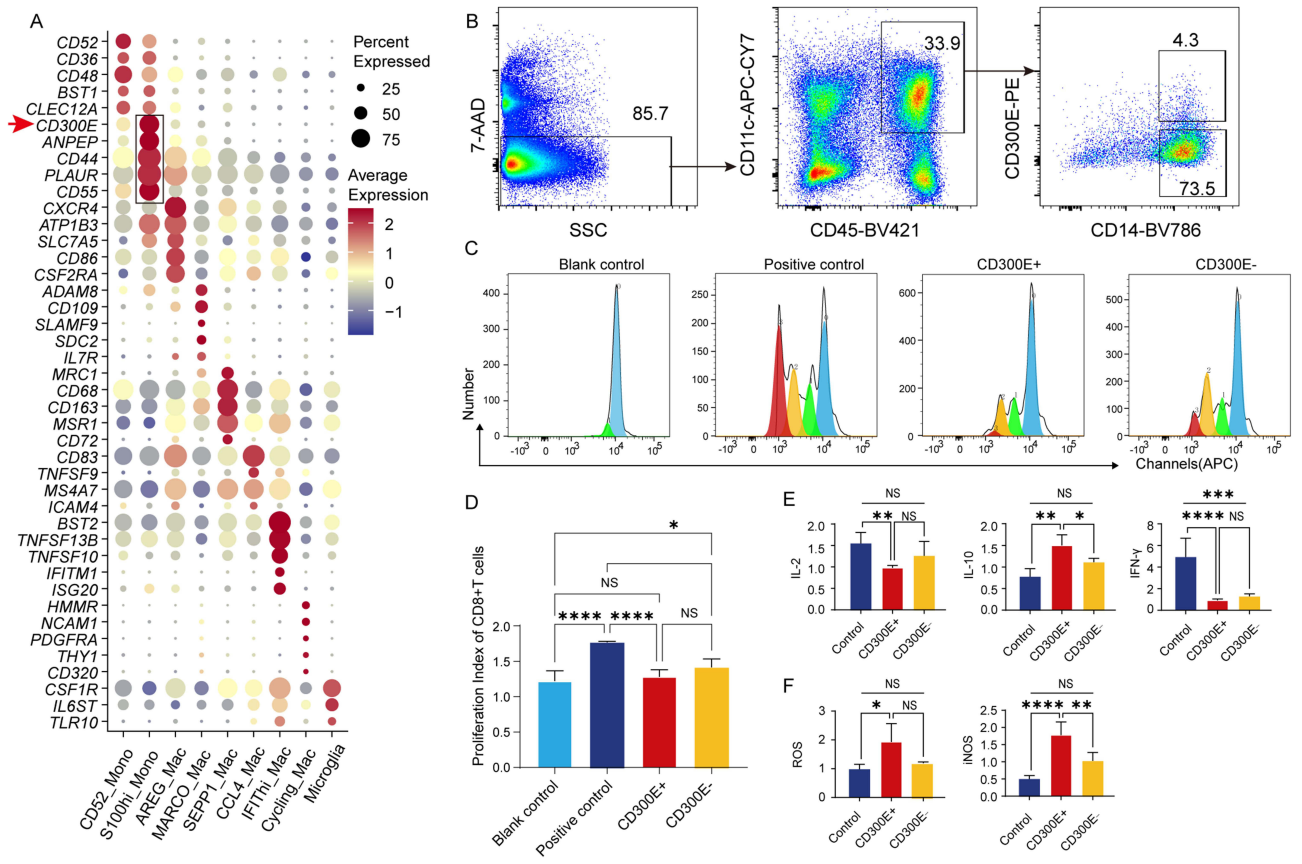

Figure 7 The immunosuppressive function of S100hi_mono. (**A**) Dot plot showing Top 5 differently expressed surface marker for each monocyte and macrophage sub-cluster. The red arrow indicates the gene CD300E was selected as a signature gene for S100hi_Mono and used for subsequent sorting. (**B**) Representative flow sorting graphs for S100hi_Mono. (**C**) eFluor450 proliferation exhibitions of CD8+ T cells in co-culture system. (**D**) Comparative analysis of T cell proliferation index among groups. (**E**) Bar plots showing the levels of indicated cytokine. (**F**) Bar plots showing the levels of ROS and iNOS. Among which, the statistical significance symbols in panels D, E, and F are defined as follows: *P ≤ 0.05; **P ≤ 0.01; ***P ≤ 0.001; ****P ≤ 0.0001; NS: P > 0.05.

resident or skull-derived myeloid immune cells have been demonstrated to be the predominant immune cells in glioma. Tumor-associated microglia, tumor-associated macrophages, and myeloid-derived immunosuppressive cells have been confirmed to play important roles in inducing the immunosuppressive microenvironment of glioma.[26,27] However, the heterogeneity of these myeloid-derived immunosuppressive cells remains to be precisely delineated.

In this study, on the basis of the expression of ligand and receptor genes, we have classified patients with gliomas into three subtypes. The C1 group displayed low expression of both ligand and receptor signaling, representing a glioma subtype with limited communication with tumors. The C2 sub-type is mainly enriched in signals related to neuron development, mightly representing a favourable communicating tumor. Intriguingly, the C3 group is enriched in immunosuppressive and angiogenesis-promoting signals, representing a nonfavourable communicating tumor type. Previous molecular classifications of glioma have mostly been based on genomic, epigenomic, and transcriptomic levels.[28] This is the first time that intercellular communication has been used alone to stratify glioma patients, emphasizing that the tumor and microenvironment function as an integrated whole. Tumor progression depends not only on the evolution of the tumor itself but also on the cooperation of the tumor microenvironment.

In addition to the high proportion of myeloid immune cells, T cells and NK cells in C3 exhibit obvious immune hyporesponsiveness state, suggestive of its immunosuppressive environment.[29,30] Through precise analysis of single-cell transcriptomic data, we discovered that the immunosuppressive microenvironment of the C3 subgroup may be closely associated with S100A9^{high} monocytes. Although S100A9 has been reported to be highly expressed in tumor-associated macrophages and neutrophil-like MDSCs, its expression and role in monocytes remain relatively poorly understood.[27,31] Therefore, this study expands our understanding of immunosuppressive myeloid cells in glioma. The high expression of

https://doi.org/10.2147/OTT.S553018

S100A9 may prevent monocytes from differentiating into mature macrophages, instead causing them to remain in an immature monocyte state or transform into monocyte-like MDSCs.[32] We also found that these immunosuppressive monocytes specifically express CD300E, an important feature of immune activation, highlighting the diverse roles of CD300E and its potential as a new therapeutic target. Mechanistically, we observed that this group of immunosuppressive monocytes highly secretes immunosuppressive cytokines such as IL10 and iNOS but does not exhibit high expression of ROS, suggesting that their immunosuppressive function may primarily rely on the former.[27] These cytokines have previously been reported to play important roles in inducing the generation of immunosuppressive macrophages and regulatory T cells, as well as in the exhaustion of cytotoxic T cells.[29,30] However, whether S100A9^{high} monocytes depend on IL10 and iNOS to exert their effects requires further validation in future studies. Furthermore, through cell-cell interaction analysis, we found that S100A9^{high} monocytes may promote tumor progression through multiple pathways. In addition to releasing immunosuppressive cytokines to construct an immunosuppressive microenvironment, they may also facilitate the generation of tumor-associated endothelial cells. Inhibiting tumor angiogenesis and reversing the immunosuppressive microenvironment are critical strategies for glioma treatment. Bevacizumab plays a significant role in anti-angiogenic therapy by targeting VEGF. Given the multiple roles of S100A9^{high} monocytes in promoting tumor progression, particularly their important functions in inducing the immunosuppressive microenvironment and generating tumor-associated endothelial cells, targeting the S100A9^{high} monocyte population in the future may achieve the effect of "killing two birds with one stone".[32] Additionally, despite the critical role of S100A9^{high} monocytes in promoting tumor development, the origin of these immunosuppressive monocytes remains unclear. Elucidating their origin and transformation pathways is not only of great significance for understanding the developmental origins of tumor-associated myeloid cells but also holds practical importance for identifying new approaches for early tumor intervention. The rapid development of single-cell genomic technologies, along with advancements in lineage tracing technologies represented by mitochondrial genome mutations, will undoubtedly provide essential technical support for deciphering the cellular origins and evolutionary patterns of these critical cell populations.[33–35]

Abbreviations

GBM, glioblastoma; ROS, reactive oxygen species; iNOS, inducible nitric oxide synthase; WHO, World Health Organization; TME, tumor microenvironment; DEGs, differentially expressed genes; PCA, principal component analysis; t-SNE, t-distributed stochastic neighbor embedding; MDSC, myeloid derived suppressive cells; Treg, regulatory T cells; TAM, tumor-associated macrophages; cDC, conventional dendritic cell; pDC, plasmacytoid dendritic cells; TP53, tumor protein 53; PTEN, phosphatase and tensin homolog.

Data Sharing Statement

The ST and scRNA-seq data supporting the results of this study can be accessed at the China National Genomics Data Center with accession codes HRA004677 and CRA011176. The datasets presented in this study can be download from Xena database and Figshare database: https://doi.org/10.6084/m9.figshare.22434341.

Ethics Approval and Consent to Participate

Informed consent was obtained from all patients who provided tissues. This study was approved by the ethics committee of PLA general hospital before the study began (S2021-610-01), and was conducted in compliance with the guidelines of the Declaration of Helsinki.

Author Contributions

XH designed and supervised the study, contributing to the conception and study design; XL, YQ, PG, HW, YL, and LR analyzed the data and wrote the manuscript, contributing to data analysis, interpretation, and drafting the work; DW collected the samples, contributing to data acquisition. All authors made a significant contribution to the work reported, whether that is in the conception, study design, execution, acquisition of data, analysis and interpretation, or in all these areas; took part in drafting, revising or critically reviewing the article; gave final approval of the version to be published; have agreed on the journal to which the article has been submitted; and agree to be accountable for all aspects of the work.

Funding

This research was funded by the National Natural Science Foundation of China (Grant No. 52473271).

Disclosure

The authors declare that the research was conducted in the absence of any commercial or financial relationships that could be construed as a potential conflict of interest.

References

1. Chen R, Smith-Cohn M, Cohen AL, Colman H. Glioma subclassifications and their clinical significance. *Neurotherapeutics*. 2017;14(2):284–297. doi:10.1007/s13311-017-0519-x
2. Jin MZ, Jin WL. The updated landscape of tumor microenvironment and drug repurposing. *Signal Transduct Target Ther*. 2020;5(1):166. doi:10.1038/s41392-020-00280-x
3. Bian Z, Gong Y, Huang T, et al. Deciphering human macrophage development at single-cell resolution. *Nature*. 2020;582(7813):571–576. doi:10.1038/s41586-020-2316-7
4. You G, Zhang M, Bian Z, et al. Decoding lymphomyeloid divergence and immune hyporesponsiveness in G-CSF-primed human bone marrow by single-cell RNA-seq. *Cell Discov*. 2022;8(1):59. doi:10.1038/s41421-022-00417-y
5. Tang F, Li J, Qi L, et al. A pan-cancer single-cell panorama of human natural killer cells. *Cell*. 2023;186(19):4235–4251.e20. doi:10.1016/j.cell.2023.07.034
6. Śledzińska P, Bebyn MG, Furtak J, Kowalewski J, Lewandowska MA. Prognostic and predictive biomarkers in gliomas. *Int J Mol Sci*. 2021;22(19):10373. doi:10.3390/ijms221910373
7. Liu C, Zhang M, Yan X, et al. Single-cell dissection of cellular and molecular features underlying human cervical squamous cell carcinoma initiation and progression. *Sci Adv*. 2023;9(4):eadd8977. doi:10.1126/sciadv.add8977
8. Liu C, Gong Y, Zhang H, et al. Delineating spatiotemporal and hierarchical development of human fetal innate lymphoid cells. *Cell Res*. 2021;31(10):1106–1122. doi:10.1038/s41422-021-00529-2
9. Zeng Y, Liu C, Gong Y, et al. Single-cell RNA sequencing resolves spatiotemporal development of pre-thymic lymphoid progenitors and thymus organogenesis in human embryos. *Immunity*. 2019;51(5):930–948.e6. doi:10.1016/j.immuni.2019.09.008
10. Popescu DM, Botting RA, Stephenson E, et al. Decoding human fetal liver haematopoiesis. *Nature*. 2019;574(7778):365–371. doi:10.1038/s41586-019-1652-y
11. Ramilowski JA, Goldberg T, Harshbarger J, et al. A draft network of ligand-receptor-mediated multicellular signalling in human. *Nat Commun*. 2015;6:7866. doi:10.1038/ncomms8866
12. Wu T, Hu E, Xu S, et al. clusterProfiler 4.0: a universal enrichment tool for interpreting omics data. *Innovation*. 2021;2(3):100141. doi:10.1016/j.xinn.2021.100141
13. Hänzelmann S, Castelo R, Guinney J. GSVA: gene set variation analysis for microarray and RNA-seq data. *BMC Bioinf*. 2013;14:7. doi:10.1186/1471-2105-14-7
14. Zeng D, Ye Z, Shen R, et al. IOBR: multi-omics immuno-oncology biological research to decode tumor microenvironment and signatures. *Front Immunol*. 2021;12:687975. doi:10.3389/fimmu.2021.687975
15. Mei Y, Wang X, Zhang J, et al. Siglec-9 acts as an immune-checkpoint molecule on macrophages in glioblastoma, restricting T-cell priming and immunotherapy response. *Nat Cancer*. 2023;4(9):1273–1291. doi:10.1038/s43018-023-00598-9
16. Jin S, Guerrero-Juarez CF, Zhang L, et al. Inference and analysis of cell-cell communication using CellChat. *Nat Commun*. 2021;12(1):1088. doi:10.1038/s41467-021-21246-9
17. Yuan H, Yan M, Zhang G, et al. CancerSEA: a cancer single-cell state atlas. *Nucleic Acids Res*. 2019;47(D1):D900–D908. doi:10.1093/nar/gky939
18. Bill R, Wirapati P, Messemaker M, et al. CXCL9: SPP1 macrophage polarity identifies a network of cellular programs that control human cancers. *Science*. 2023;381(6657):515–524. doi:10.1126/science.ade2292
19. Derynck R, Turley SJ, Akhurst RJ. TGFβ biology in cancer progression and immunotherapy. *Nat Rev Clin Oncol*. 2021;18(1):9–34. doi:10.1038/s41571-020-0403-1
20. Glorieux C, Liu S, Trachootham D, Huang P. Targeting ROS in cancer: rationale and strategies. *Nat Rev Drug Discov*. 2024;23(8):583–606. doi:10.1038/s41573-024-00979-4
21. Akkari L, Amit I, Bronte V, et al. Defining myeloid-derived suppressor cells. *Nat Rev Immunol*. 2024;24(12):850–857. doi:10.1038/s41577-024-01062-0
22. Kumagai S, Itahashi K, Nishikawa H. Regulatory T cell-mediated immunosuppression orchestrated by cancer: towards an immuno-genomic paradigm for precision medicine. *Nat Rev Clin Oncol*. 2024;21(5):337–353. doi:10.1038/s41571-024-00870-6
23. Colonna M. The biology of TREM receptors. *Nat Rev Immunol*. 2023;23(9):580–594. doi:10.1038/s41577-023-00837-1
24. Wu Y, Ma J, Yang X, et al. Neutrophil profiling illuminates anti-tumor antigen-presenting potency. *Cell*. 2024;187(6):1422–1439.e24. doi:10.1016/j.cell.2024.02.005
25. Tran TO, Lam LHT, Le NQK. Hyper-methylation of ABCG1 as an epigenetics biomarker in non-small cell lung cancer. *Funct Integr Genomics*. 2023;23(3):256. doi:10.1007/s10142-023-01185-y
26. Quail DF, Joyce JA. The microenvironmental landscape of brain tumors. *Cancer Cell*. 2017;31(3):326–341. doi:10.1016/j.ccell.2017.02.009
27. Nakamura K, Smyth MJ. Myeloid immunosuppression and immune checkpoints in the tumor microenvironment. *Cell Mol Immunol*. 2020;17(1):1–12. doi:10.1038/s41423-019-0306-1
28. Yi Z, Song M, Liang L, et al. Comprehensive multi-omics approach reveals critical genes and immunometabolic networks in glioblastoma. *Int J Surg*. 2025;111(8):5137–5149. doi:10.1097/JS9.0000000000002634

29. Yang Y, Wang F, Zhang Y, et al. Comprehensive characterization of the immune microenvironment based on nested resampling machine learning framework identifies TRAF3 interacting protein 3 as a promising regulator to improve the resistance to immunotherapy in glioma. *Adv Sci (Weinh)*. 2025;12(35):e02271. doi:10.1002/advs.202502271
30. Qiao A, Zhang Q, He J, et al. Cell division cycle 25 C (CDC25C) mediates cell-cycle progression and immune evasion in glioma. *Discov Oncol*. 2025;16(1):1779. doi:10.1007/s12672-025-03596-8
31. Veglia F, Sanseviero E, Gabrilovich DI. Myeloid-derived suppressor cells in the era of increasing myeloid cell diversity. *Nat Rev Immunol*. 2021;21(8):485–498. doi:10.1038/s41577-020-00490-y
32. Chai H, Xu H, Jiang S, et al. Neural stem cell-delivered oncolytic virus via intracerebroventricular administration enhances glioblastoma therapy and immune modulation. *J Immunother Cancer*. 2025;13(10):e012934. doi:10.1136/jitc-2025-012934
33. Li J, Yu X, Yang D, et al. Lipid-metabolically active TREM2high Microglia-derived macrophages predict poor prognosis and represent an immunotherapeutic target in glioma. *J Neuroimmune Pharmacol*. 2025;20(1):92. doi:10.1007/s11481-025-10250-1
34. Andrade AF, Sigaud R, Puligandla E, et al. A spatial map of MAPK-activated immunosuppressive myeloid populations in pediatric low-grade glioma. *Nat Immunol*. 2025;26(10):1794–1806. doi:10.1038/s41590-025-02268-7
35. Bancaro N, Calì B, Troiani M, et al. Apolipoprotein E induces pathogenic senescent-like myeloid cells in prostate cancer. *Cancer Cell*. 2023;41(3):602–619.e11. doi:10.1016/j.ccell.2023.02.004